 CMES, vol.120, no.1, pp.157-175, 2019

Numerical Simulation of Derusting Treatment of Steel Parts By Shot Blast

Zhe Li[1], Fan Yang[1,*], Yaping Liu[1] and Yukui Gao[1]

Abstract: In this paper, we investigated the shot blast treatment for derusting application through finite element (FE) simulations with a large number of random shots. The element deletion technique based on dynamic failure criteria was used to model the removal of rust. The cohesive surface model with damage evolution was used to characterize the decohesion of the rust/substrate interface. The effects of various processing and material parameters on the derusting effectiveness were examined. The results show that the rate of derusting mainly depends on the shot size, velocity and impinging angle, with little relevance to the rust thickness. The spalling of the rust fragments resulted from the decohesion of the rust/substrate interface were observed, especially during the later stage of the treatment. Furthermore, the residual stress and the surface roughness was also investigated and the beneficial effects of shot blast treatment in terms of these aspects were highlighted.

Keywords: Shot blast, rust removal, cohesive surface, finite element.

1 Introduction

Metal rusting is a common issue in industry that can cause degradation of the surface, shortening of the service life of components, and thus a significant economic loss. On the other hand, remanufacturing and recycling have attracted increasing interest in both academic and industrial communities. Proper cleaning of the oxidation contaminant is often a critical step for the accomplishment of the subsequent recycling processes. Therefore, it is of practical importance to investigate how to clean metal oxide effectively and economically for the sake of recycling metal parts.

A number of techniques have been developed for this purpose. Abrasive water jets (AWJs) has been successfully applied for rust removal [Kumar and Shukla (2012); Junkar, Jurisevic, Fajdiga et al. (2006)]. The influences of impact angle and velocity on the erosion rate have been investigated. A model for AWJs processing [Lebar and Junkar (2003)] was developed to forecast the workpiece topography, in order to examine the adverse influences of scratches inevitably left on the surface of workpiece during this treatment. The second approach is using chemical derusting. Brannon et al. [Brannon and Asmus (1981)] repeatedly dissolved the rust by using citric acid flash cleaning for many cycles which is able to retard the corrosion. Lu et al. [Lu, Brooks, Chen et al. (2005)]

[1] School of Aerospace Engineering and Applied Mechanics, Tongji University, Shanghai, 200092, China.

[*] Corresponding Author: Fan Yang. Email: fanyang@tongji.edu.cn.

proposed a cleaning technique to clean the oxidized sample by an alkaline solution after a boiling treatment, which has the advantage of maintaining the fracture surface morphology. Attention has also been paid to the pulsed laser cleaning. Oltra et al. [Oltra, Yavas, Cruz et al. (1996)] demonstrated the mechanisms of the pulsed laser cleaning and developed a new approach to deal with reoxidation. Wang et al. [Wang, Zeng and Huang (2003)] studied the effects of laser parameters on the performance of derusting and the roughness of the cleaned surfaces.

Until now, in spite of the various approaches mentioned above, shot blast is still one of the most widely used approaches for derusting. This is probably attributed to its high efficiency, high flexibility and low cost. In addition, shot blast can extend the fatigue life of the treated metallic components due to the introduction of compressive residual stresses near the component surface [Gao and Wu (2011); Guagliano (2001)]. The increased roughness resulted from the treatment [Mylonas and Labeas (2011); Unal (2016)] can enhance the adhesion of the paint to the surface which is beneficial for the following processing steps. These advantages guarantee shot blast as a competitive choice for cleaning rust in the short run. In this paper, we focused on the numerical simulations of derusting by shot blast.

A number of experiments have been carried out to explore the mechanisms of coating removal by solid particles. Papini et al. [Papini and Spelt (1997)] investigated the spallation by stress waves and delamination by shear stresses, and then developed a theoretical model [Papini and Spelt (1998a); (1998b)] for the buckling and delamination of organic coating caused by particle impact. Further investigation [Papini and Spelt (1998c)] showed organic coatings would be removed by particle erosion in the case of a sufficiently strong interface between the coating and the substrate. Shipway et al. [Shipway, Bromley and Weston (2007)] pointed out that paint removal by particle blasting would be effective for the chrome/ABS system, while would be less efficient for a compliant coating/substrate system such as the paint coatings on polypropylene substrates. In addition, Li et al. [Li, Liu, Qing, et al. (2016)] proposed a pretreatment using supercritical CO_2 followed by wet blasting for paint cleaning. Numerical simulation is a useful tool for investigating the process of various mechanical treatments, but the large number of shots involved in the shot blasting treatment placed a big challenge for this approach. In recent years, numerical simulation of shot peening using finite element method and discrete element method has received increasing attention thanks to the development of computing power. Representative cell models utilizing symmetric [Meguid, Shagal and Stranart (2002)] or periodic boundaries [Yang, Chen and Meguid (2014); Yang, Chen and Meguid (2015)] were developed to study the effect of various processing or material parameters such as the incident velocity, angle and initial surface roughness on the effectiveness of shot peening. These models are efficient in computation, but will introduce boundary effects in the obtained results. Wang et al. [Wang and Yang (2008); Griffin, Daadbin and Datta (2004)] utilized element removal technique to simulate the erosive behavior of both brittle and ductile materials. Zouari et al. [Zouari and Touratier (2002)] used paint removal model considering interface damage based on traction-separation relationship to simulate the interfacial debonding process. These numerical researches provide insights into the material response under shot impingements. However, for the specific problem of derusting by shot blast, hardly any

numerical simulation efforts can be found in the literature. The reason may be attributed to the vast computational demand for simulating the shot blast treatment that involved considerable number of parameters. Recent progress in computing power of supercomputers provides possibility for the simulation of this complex process.

In this paper, we aim at investigating the shot blast treatment for derusting through FE numerical simulations on supercomputers. Both the material erosion based on the elemental dynamic failure model and the rust/substrate interface decohesion based on the cohesive surface model with damage evolution are incorporated in the simulations. The paper is organized as follows. Following this introduction, the details of the FE model as well as its validation are presented in Section 2. Section 3 gives the results of an extensive parametric study on the effects of various parameters on the treatment effectiveness. Section 4 concludes the paper.

2 Finite element modelling

2.1 Geometry, boundary condition and material models

The 3D finite element model was developed using the generalized FE code ABAQUS Explicit version 6.14 [Abaqus (2014)]. The model contains a half-plate steel substrate coated with the oxide layer, which was impacted by a large number of shots at the surface. Fig. 1 shows the discretized FE model with different colors indicating different regions. The blue region represents the steel substrate with dimensions: diameter $D_{\text{sub}} = 10D$, thickness $H_{\text{sub}} = 2D$, where D is the shot diameter. On the top of the substrate is the rust coating colored with gray. At the center of the rust region there is a red mesh-refined region with length $L_{\text{cen}} = 3D$, width $W_{\text{cen}} = 1.5D$, and approximate element size of $0.15D$. This region was the treated region from which the statistics of the simulation results were obtained. At the outskirts of the half-plate model there is a ring of infinite elements (type CIN3D8, color green, radius $R_{\text{inf}} = 10D$) to avoid the reflection of stress waves at the boundaries in order to shield the boundary effect. The material properties of the outskirt region only include the elastic part of the corresponding material models, according to the usage of infinite elements [Abaqus (2014)]. The thickness of the plate is also sufficiently large to neglect the effect of the bottom boundary on the simulation results according to Meguid et al. [Meguid, Shagal and Stranart (2002)].

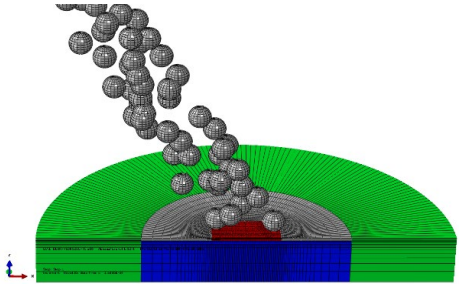

Figure 1: FE model

The substrate was modeled using the von Mises elasto-plastic law of bilinear stress-strain relation, with elastic modulus E_1 =200 GPa, Poisson's ratio ν_1 =0.3, density ρ_1 =7800 kg/ m^3 , initial yield stress σ_1^0 =1120 MPa. The strain-rate sensitivity was accounted for by using the data developed by Premack et al. [Premack and Douglas (1995)]. The detailed material parameters can refer to the Meguid et al. [Meguid, Shagal and Stranart (2002)].

Mechanical properties of rust are difficult to be determined. According to Nguyen et al. [Nguyen, Bary and De Larrard (2015)], the elastic modulus of the steel oxidation ranges from 0.1 to 350 GPa. The vast deviation comes from the varying composition, compaction and hydration of the rust material. Ouglova et al. [Ouglova, Berthaud, Francois et al. (2006)] showed that the oxide layer mainly consists of goethite (γ FeO(OH)), lepidocrocite (γ FeO(OH)), maghemite (Fe_2O_3). Since the naturally formed rust is usually an aggregate of powder grains, it has a much less mechanical stiffness than its compacted counterpart. In this work, the elastic modulus of the rust is set to be 6 GPa [Ouglova, Berthaud, Francois et al. (2006)]. Other material properties are: ρ_2=2345 kg/ m^3 , ν_2=0.2. The ultimate tensile strength is determined indirectly as follows. According to fracture mechanics,

$$\sigma_c = \frac{K_c}{\sqrt{\pi a}} \tag{1}$$

where, a is the crack length, σ_c is the critical fracture stress, and K_c is the critical fracture toughness of the rust. From Ouglova et al. [Ouglova, Berthaud, Francois et al. (2006); Zhang, Ma, Wu et al. (2002)], K_c=2.60 MPa·m$^{0.5}$, a =3.35 μm. Therefore, σ_c is calculated as 802 MPa.

The element deletion technique based on dynamic failure criterion was used to simulate the erosion of the rust material. A damage variable ω was introduced as being:

$$\omega = \frac{\sum \Delta \bar{\varepsilon}^{pl}}{\bar{\varepsilon}_f^{pl}} \tag{2}$$

where, $\Delta \bar{\varepsilon}^{pl} = \sqrt{\frac{2}{3} \Delta \boldsymbol{\varepsilon}^{pl} : \Delta \boldsymbol{\varepsilon}^{pl}}$ is the equivalent plastic strain increment, $\bar{\varepsilon}_f^{pl}$ is the critical plastic strain for failure. Since the rust is a brittle material, $\bar{\varepsilon}_f^{pl}$ is set to small value of 0.001. An element with ω=1.0 is considered to be fully failed, and is deleted from the simulation thereafter.

The shots were modeled as rigid analytical spheres with the same density as the steel substrate, and initially placed above the target with specified velocities directing towards the target surface. The initial positions of the shots followed the pattern that the shots impinge randomly at the target surface with an interval of 3 μs between subsequent impingements. Contact algorithm was established between the shots and the rust top surface. During the simulation, the contacts between the shots and the rust interior surface, between the shots and the substrate surface, as well as between the rust

interior surface and itself were also taken into account to model the progressive procedure of rust removal. The friction coefficients are unanimously set to 0.3 according to literature [KIM, Lee, Hyun et al. (2003)]. The collisions between shots are not considered in this work for simplicity.

Symmetric boundary condition is applied to the cutting side face of the target. Constrained boundary condition is applied to the bottom of target to avoid rigid body movements. In order to avoid numerical instability, material damping was introduced with the damping matrix C expressed as:

$$C = \alpha M + \beta K \tag{3}$$

where M and K are the mass and stiffness matrices, respectively. As recommended by Meguid et al. [Meguid, Shagal and Stranart (2002)], the stiffness proportional and mass proportional damping coefficients took the values of:

$$\beta = 2\times10^{-9}s\,,\ \alpha = \frac{2\zeta}{H}\sqrt{\frac{2E}{\rho}} \tag{4}$$

where, E is targets Young's modulus , ρ is target's density and H is thickness of model. ζ is a dimensionless coefficient specified as 0.5.

The cohesive zone model [Park and Paulino (2011); Diehl (2008a); Diehl (2008b); Karac, Blackman, Cooper et al. (2011)] has been widely used to analyze crack initiation and propagation at the interface. In the current work, we applied the surface based cohesive zone model [Ramamurthi, Lee, Yang et al. (2013)] to simulate the de-bonding of the interface between the target and oxide layer. The damage initiation criterion is given as

$$\left\{\frac{\langle t_n\rangle}{t_n^0}\right\}^2 + \left\{\frac{\langle t_s\rangle}{t_s^0}\right\}^2 + \left\{\frac{\langle t_t\rangle}{t_t^0}\right\}^2 = 1 \tag{5}$$

where, t_n^0, t_s^0 and t_t^0 represent the critical values of the cohesive stress for damage initiation in the normal direction, the first, and the second shear direction, respectively.

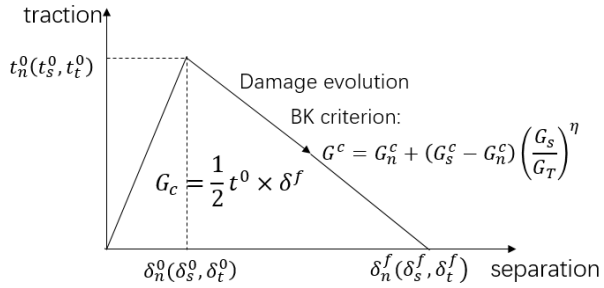

Figure 2: Surface-based cohesive behavior

Damage evolution was given by the BK mixed mode law (Fig. 2). For the isotropic condition, only two independent parameters are included in the model [Diehl (2008a)]: the interfacial fracture energy G_c and the interfacial cohesive strength $T_{\text{ult}} = t_n^0 = t_s^0 = t_t^0$. G_c can be determined by using the tests of double cantilever beam or tapered double cantilever beam [Blackman and Kinloch (2001)]. However, such tests are difficult to carry out and the obtained results are highly scattered [Diehl (2008a)]. Here, we estimated G_c via the fracture toughness K_{IC} using the following equations [Banks-Sills (2015)]:

$$G = J = \frac{1}{2E^* Ch^2(\pi\varepsilon)}\left|K_{IC}\right|^2 \tag{6}$$

$$\frac{1}{E^*} = \frac{1}{E_1} + \frac{1}{E_2} \tag{7}$$

$$\varepsilon = \frac{1}{2\pi}\ln\left[\left(\frac{\chi_1}{\mu_1} + \frac{1}{\mu_2}\right)\Big/\left(\frac{\chi_2}{\mu_2} + \frac{1}{\mu_1}\right)\right] \tag{8}$$

where, E_i, μ_i and ν_i (i=1,2) are the ith material's Young's modulus, shear modulus and Poisson's ratio, respectively. For the plane strain case, $\chi_i = 3 - 4\nu_i$

From the literature [Zhang, Ma, Wu et al. (2002)], [28] K_{IC}=2.60 MPa· $\text{m}^{0.5}$. Therefore, G_{c} is estimated as 506 N/m.

2.2 Validation of the FE model

For comparison purpose, we conducted a shot blasting experiment on a rusted steel plate to examine the derusting efficiency. The specimen was cut down from an obsolete farming machine, and was exposed to outdoor environment near Datong, Shanxi Province (Longitude 113° E, Latitude 40° N) for four years before test. The oxidation was uniformly distributed at the surface on both sides of the plate. Fig. 3(a) shows an enlarged view of the rusted surface, obtained using an optical microscope. The specimen has a size of 200×250 mm and a thickness of 1.25 mm. The specimen was first cut into two equal pieces. Each piece was shot blasted using the same test parameters. In this way, two set of test data can be obtained to testify the repeatability. The thickness of the oxide layer is about 0.1 mm at both sides of surface. The oxide thickness was estimated by measuring the thickness of the specimen before and after the derusting test using a micrometer.

The shot blasting tests were carried out at Shanghai Shili Machineries Co. using a cabinet shot-blasting machine of model Kaitech QY360. The specimen was fixed on a supporter inside the cabinet and blasted by the hard-steel shot media of S110 [Society of Automotive Engineers (2001)], which has a diameter D of 0.2 mm. The shot media is accelerated by a wheel impeller with the diameter of 0.36 m and the rotating speed of 1500 r/min. The incident velocity is estimated as 78 m/s. Only one side of surface was blasted during the test and the other side was protected by covering it with a plate of the same size. Every a while (first 30 sec, then gradually extending to 10 min), the specimen was taken out of the cabinet and weighed by an electronic balance with

accuracy of 0.01 g. The mass of the removed rust was obtained from the mass loss of the specimen. Fig. 3(b) shows the morphology of the derusted specimen surface under an optical microscopy.

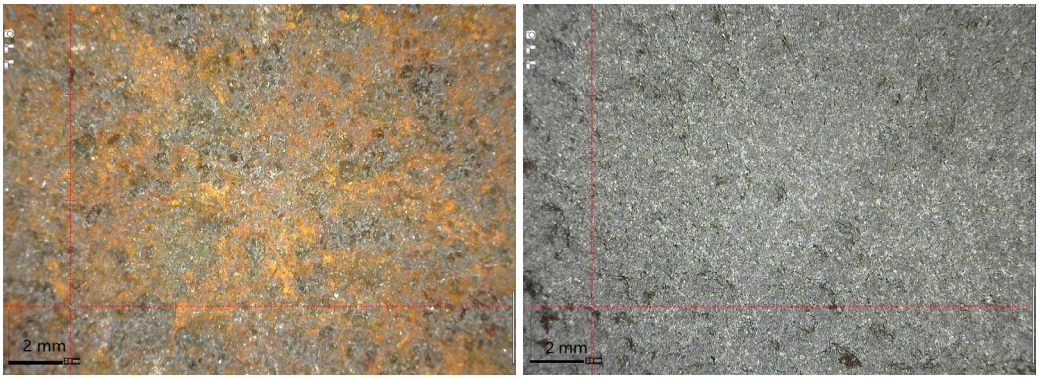

(a) (b)

Figure 3: Morphology of the specimen surface (a) before and (b) after the shot blasting treatment, obtained using an optical microscopy

For comparison, a FE simulation with the same shot size, the same incident velocity and the same oxide thickness as in the experiment was carried out. It is noted that direct simulating the entire specimen is computationally arduous and unnecessary. Our FE model utilized a small representative region (the red region in Fig. 1) to simulate the derusting process. Therefore, the data obtained from the simulations should be converted to represent the same conditions as in the tests. The removed volume V_{loss} and the accumulated number of the incident shots N from the simulations are converted to the mass loss of the specimen m_{loss} and the processing duration t, respectively, using Eq. (9) and Eq. (10).

$$m_{\text{loss}} = \rho_2 V_{\text{loss}} \frac{A_{\text{specimen}}}{A_{\text{FE}}} \tag{9}$$

$$t = \frac{N m_{\text{shot}}}{\eta \dot{M}} \frac{A_{\text{machine}}}{A_{\text{FE}}} \tag{10}$$

where, A_{FE} is the blasted area in FE simulation, A_{specimen} is the area of the specimen, $m_{\text{shot}} = \pi D^3 \rho_1 / 6$ is the mass of a single shot, $\dot{M}$ is the cycling rate of the shot media, η is the impelling efficiency, and A_{machine} is the equivalent working area inside the machine cabinet. These parameters are: D=0.2 mm, $A_{\text{FE}} = 4.5D^2$, $A_{\text{specimen}} = 0.025\ \text{m}^2$, $A_{\text{machine}} = 2\pi D_{\text{machine}}^2 / 4 = 6.28\ \text{m}^2$, $\dot{M} = 115\ \text{kg/min}$, $\eta = 0.1$.

Fig. 4 compares the removed rust obtained from the FE simulations with that obtained from the experiments. The two dot markers correspond to the two specimens tested. The difference between the simulation results and the experimental data is within

satisfactory range. The agreement between the simulated results and the experiments provides validation for our FE models.

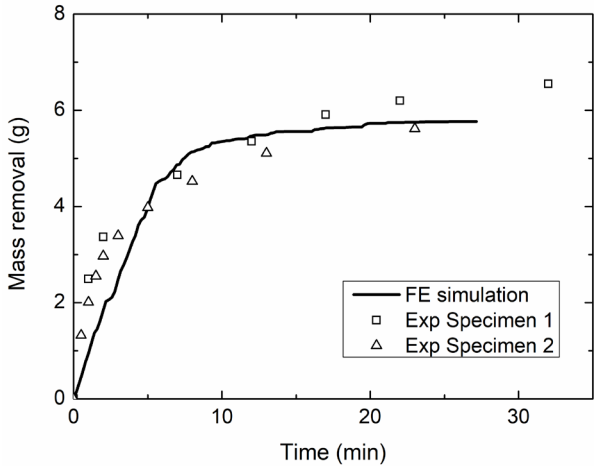

Figure 4: Comparison between experiment and FE simulation for the mass of the removed rust varying with the treatment duration

3 Results and discussions

A parametric study was carried out to investigate the effects of different processing parameters on the derusting performance of shot blast. Specifically, four aspects of the treatment effectiveness were investigated: the volume of removed rust, the ratio of damaged interface, the surface roughness, and the residual stress distribution. ABAQUS/Python scripts were developed to post-process the simulation data and get the statistical results. In this section, the involved variables are denoted as: T_{ult} interfacial cohesive strength, h rust thickness, D shot diameter, V incident velocity, V_h tangential component of velocity, θ incident angle, f interface friction coefficient, and N accumulated number of shot impingements. The benchmark simulation case was chosen as: T_{ult}=120 MPa, D=0.7 mm, h=0.1 mm, V=60 m/s, θ=90°, f=0.3, N=120.

3.1 Effect of interfacial properties

To investigate the effect of interfacial properties on the derusting behavior, we compared the results of the benchmark simulation with the case without interface failure, i.e., the rust and substrate were fully bonded at the interface. From the simulations, we observe a number of rust fragments spalled from the target as shown in Fig. 5. The total removed mass includes the part by the element failure, and the part by the spallation. The latter part can be discriminated via monitoring the velocity of each element. An ABAQUS/Python code was developed to calculate the removed rust for each removal mechanism. Fig. 6 compares the ratio of rust removal contributed only by element failure with that includes the both mechanisms. It shows that the curve corresponding to the total rust removal starts to deviate from the curve corresponding to the part contributed by element failure after 30 shot impingements, indicating that

spallation mainly took place after a certain treatment duration. Fig. 7(a) compares the ratio of the spalled volume among the models with different interface conditions. It shows that initially the spalled volume from the model with interface failure is smaller than that without interface failure. At time point of 40 shots impinged, the spalled volume for the model with interface failure witnesses an abrupt increase, which coincides with the formation of a chunk fragment spalled from the target as seen in Fig. 7(b). Therefore, the large spalled volume from the model with interface failure is attributed to the generation of chunk spallations. From the simulation results, the spallation can be further classified into two kinds: the chunk spallation and the clastic spallation. The clastic spallation comes from the non-uniformity in elemental failure caused by the non-uniform stress distribution. The chunk spallation comes from the failure of the interface between the rust and the substrate. Indeed, no chunk spallation is observed in the simulations without modeling interface failure. It also indicates from Fig. 7(a) that the chunk spallation makes a much larger contribution to the derusting than the clastic spallation. From Fig. 7(a), it also shows that the interfacial cohesive strength T_{ult} has a minor effect on the derusting.

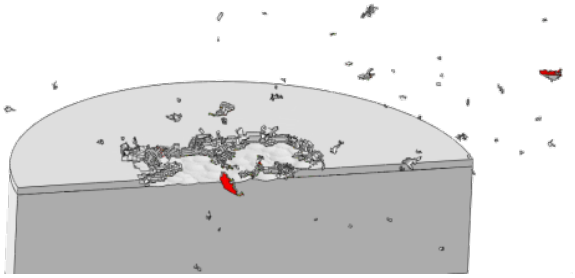

Figure 5: Spallation in two ways: chunk spallation with the damaged interface (red color indicates the damage variable at interface reaches the critical value 1) and clastic spallation

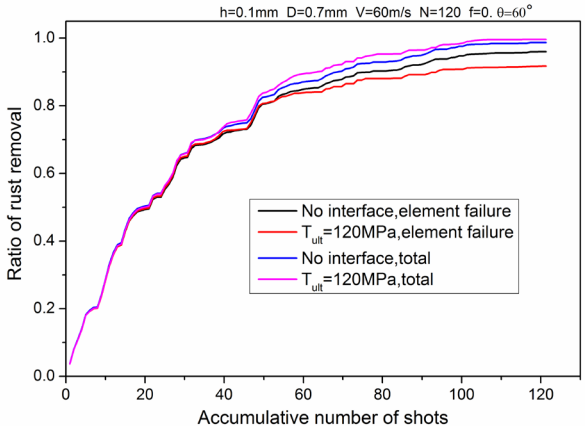

Figure 6: Element failure ratio and total ratio of rust removal

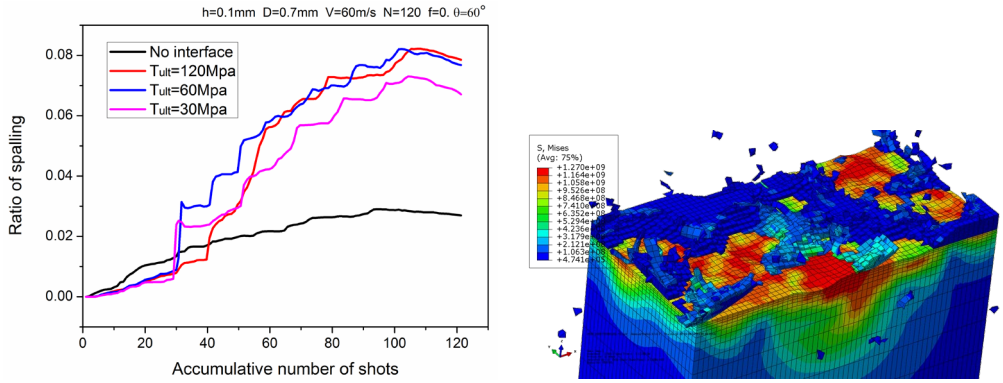

(a) (b)

Figure 7: Effect of interface on fragment spalling: (a) comparison among models with different interface conditions, and (b) chunk fragment spalled from the target

3.2 Effect of incident angle

A series of simulations with different incident angles were carried out. As shown in Fig. 8, a larger incident angle result in a higher derusting rate. Fig. 8 also indicates that the 75° incident angle leads to almost the same derusting rate as the 90° incident angle. Considering that the 75° incident angle will largely avoid the collisions between impinging shots and the rebounding shots, thus is recommended for the practical shot blast application.

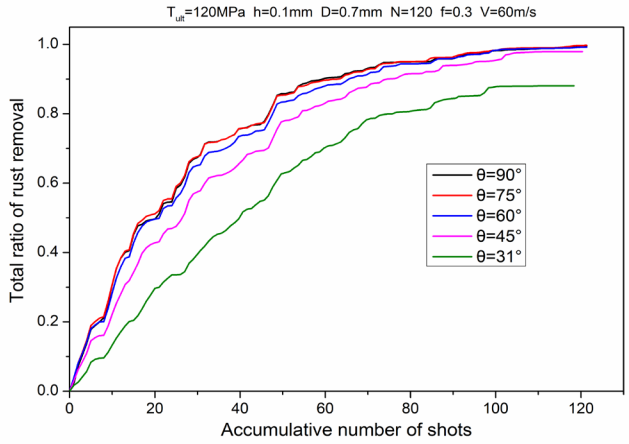

Figure 8: Effect of incident angle on derusting

If only the spalled volume is considered, the influence of incident angle is, however, contrary to that for the total removed volume. A larger incident angle results in a lower rate of spalled volume as shown in Fig. 9. The smaller spalled volume for larger incident angle can be related to the smaller ratio of failed interface as shown in Fig. 10. Fig. 11 shows the contours of the damage variable at interface. For the normal

incidence, the contours profiles are right circles. But for the oblique incidence, the contours are eccentric oblates. For normal incidence, the elements at the impinging location are removed by elemental failure mechanism before the interface reaches critical damage status, therefore leading to a smaller interface failure ratio.

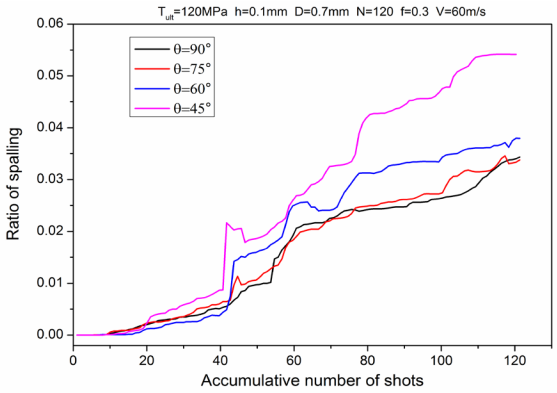

Figure 9: Variation of total spalling ratio for different incident angle

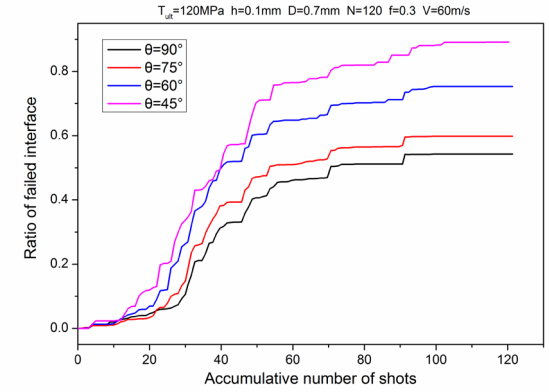

Figure 10: Effect of incident angle on interface damage

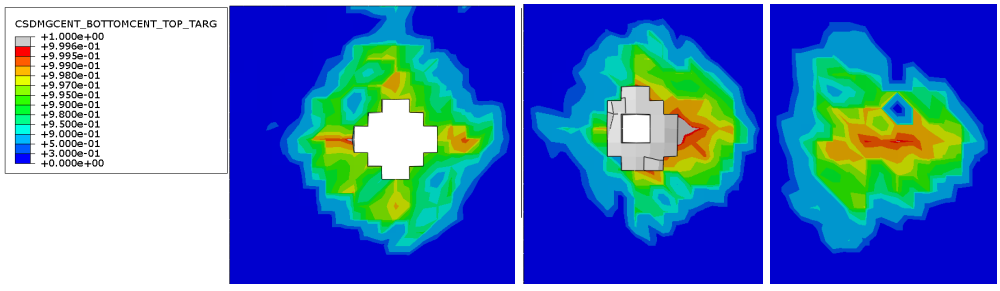

Figure 11: Contours of the damage variable for different incident angle, (Left) 90°, (middle) 60°, and (right) 45°

3.3 Effect of the incident velocity

In this section we investigate the effect of incident velocity on the derusting. Fig. 12 shows the effect of vertical velocity that is normal to the surface, and Fig. 13 for the effect of the horizontal velocity that is tangential to the surface. For both cases, the rust is removed faster as the velocity increases. The normal velocity has an obviously larger effect on the derusting than the tangential velocity.

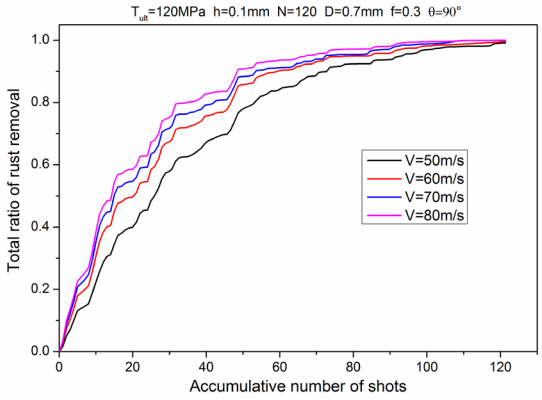

Figure 12: Effect of normal velocity on derusting

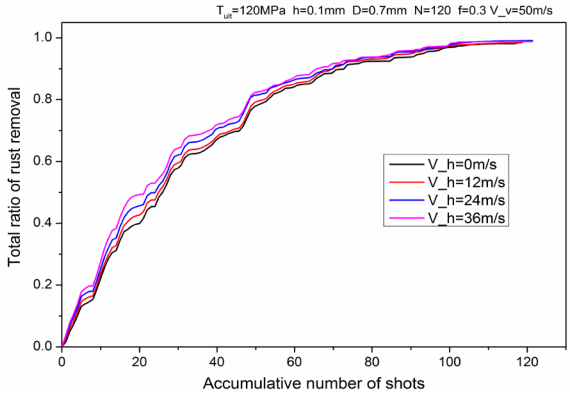

Figure 13: Effect of tangential velocity on derusting

Fig. 14 and Fig. 15 respectively show the effect of normal velocity and tangential velocity on the interface failure. For both normal and tangential velocities, the interface failure rate increases with the velocity magnitude. Different from the rust removal rate, the interface failure rate is more sensitive to the tangential velocity.

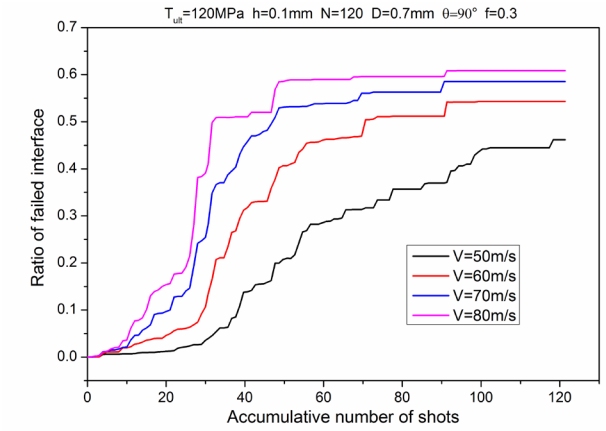

Figure 14: Effect of vertical velocity on interface failure

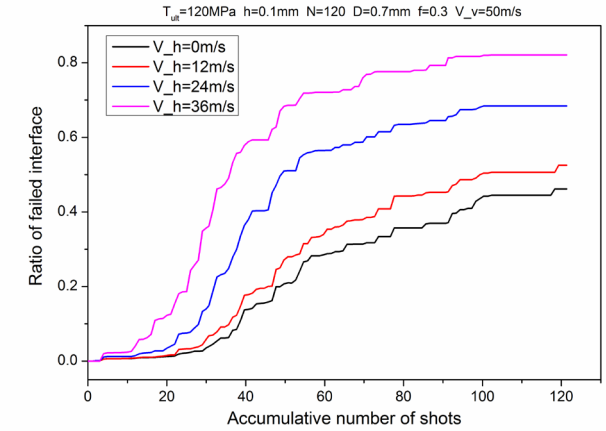

Figure 15: Effect of tangential velocity on interface failure

3.4 Effect of shot diameter

To investigate the effect of shot size on the derusting, simulations were carried out for three shot diameters: D=0.5, 0.58, and 0.70 mm [Society of Automotive Engineers (2001)]. Fig. 16 shows that the derusting rate increases with the shot diameter. Comparing with Figs. 12 and 13, it is found that rust removal rate is more sensitive to the shot diameter than to the incident velocity. This result can be probably explained if we look at the kinetic energy of the shot $K = \frac{\pi}{12}\rho D^3 V^2$, which is cubically proportional to the shot diameter, and quadratically proportional to the incident velocity. Interface failure ratio also increases faster for a larger shot diameter as shown in Fig. 17.

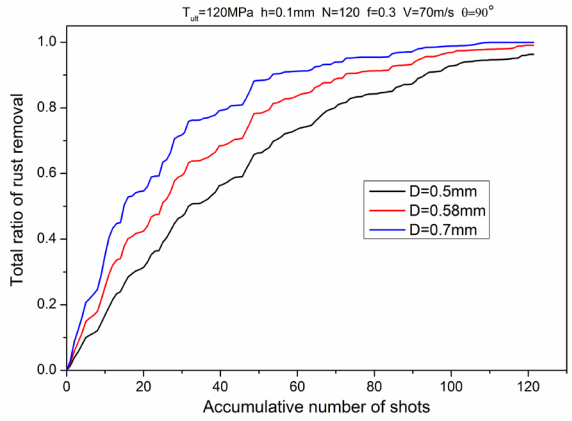

Figure 16: Effect of shot diameter on derusting

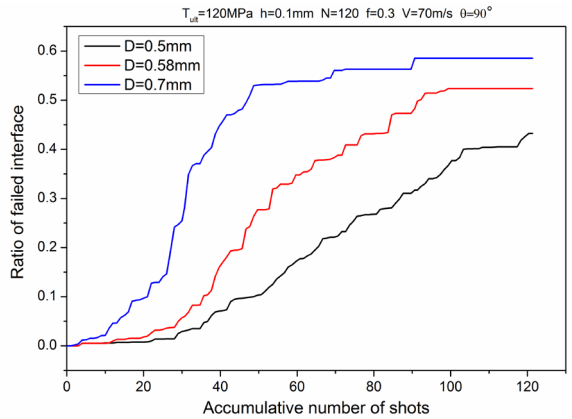

Figure 17: Effect of shot diameter on interface damage

3.5 Average roughness R_a and compressive residual stress σ_{xx}

We also investigated the effects of processing parameters including the impact velocity, incident angle and shot diameter, on the average roughness which is defined as:

$$R_a = \frac{1}{N}\sum_N \left| Z_i - \bar{Z} \right| \tag{11}$$

where N is the number of nodes being counted. Z_i is the z coordinate of the ith node on the treated surface. $\bar{Z}$ is the average of z coordinates. From Fig. 18, the roughness is larger for a higher incident velocity, and/or a larger incident angle, and/or a larger shot diameter. Comparing Fig. 18(a) with 18(b) also indicates that surface roughness is more sensitive to the vertical normal than to the tangential velocity.

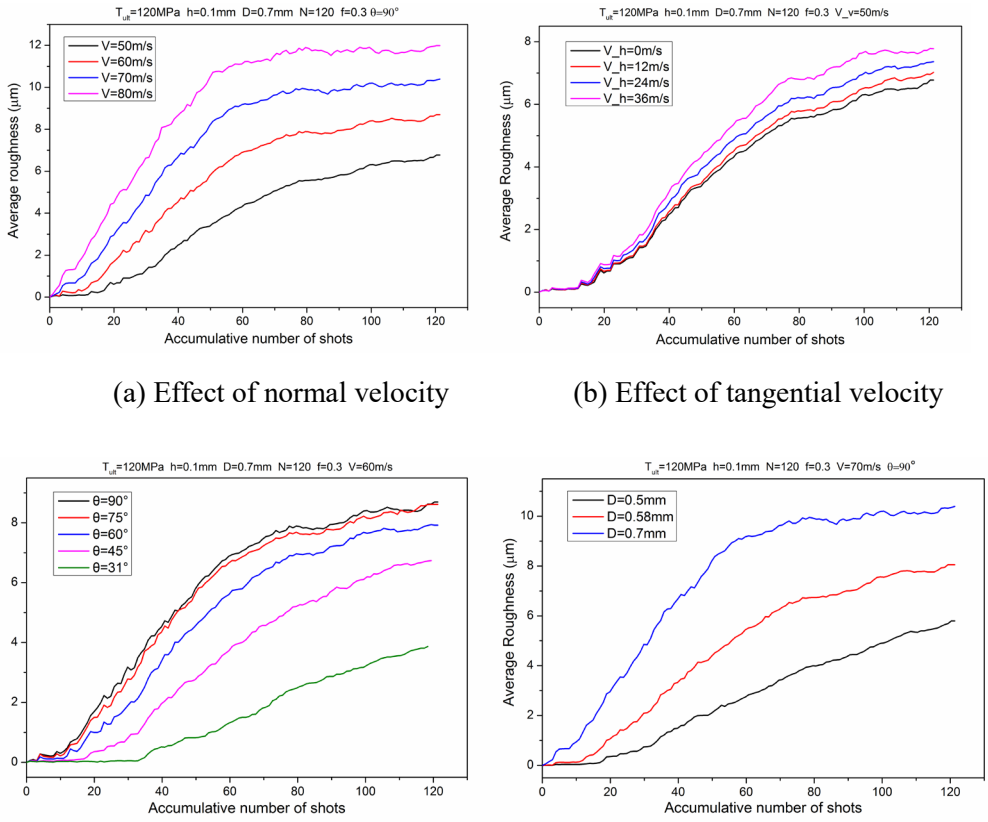

(a) Effect of normal velocity (b) Effect of tangential velocity

(c) Effect of incident angle (d) Effect of shot diameter

Figure 18: Variation of surface roughness with accumulative shots for different proceeding parameters

Compressive residual stress is a beneficial side effect of shot blast. It can effectively retard the crack growth and significantly extend the fatigue life of the working components. Fig. 19 shows the effects of different processing parameters on the distribution profile of the residual stress σ_{xx} along depth direction. To make the results of statistical significance, the residual stress σ_{xx} is averaged at each depth. An ABAQUS/Python script was developed for this computation. It shows that both the maximum residual stress and the depth of compressive stress will become larger for a higher incident velocity, and/or a larger incident angle, and/or a larger shot diameter. Comparing Figs. 19(a)-19(c), the incident angle has the most remarkable influence on residual stress among the three parameters.

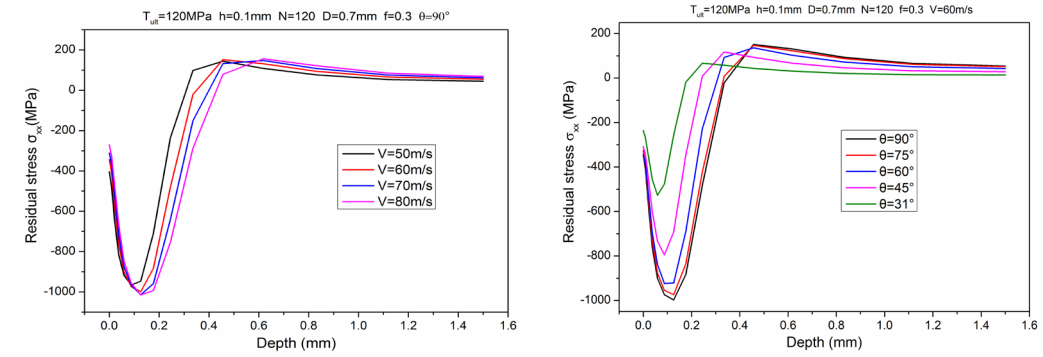

(a) Effect of impact velocity (b) Effect of incident angle

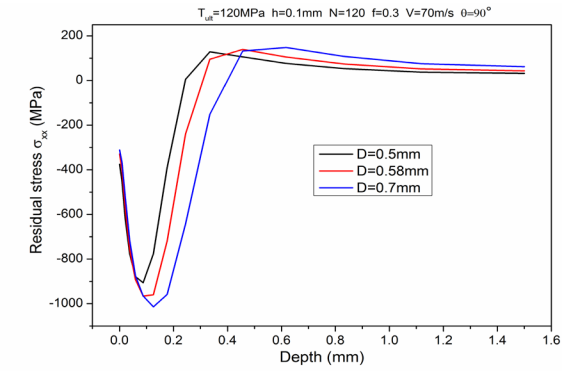

(c) Effect of shot diameter

Figure 19: Variation of residual compressive stresses σ_{xx} with depth from top surface of target under different processing parameters

4 Conclusions

In this paper, a parametric study was carried out on derusting by shot blast treatment based on realistic FE simulations with a large number of random shots. Both the material erosion and the rust/substrate interface decohesion were considered in the model based on the element deletion technique and the cohesive surface description with damage evolution. The effectiveness of shot blast treatment was examined through four aspects: the volume of removed rust, the ratio of damaged interface, the surface roughness, and the residual stress distribution. The following conclusions can be drawn from the obtained results:

(i) Spallation of rust fragments were observed in the simulations. The total rust removal is composed of the failed elements and the spalled fragments. The chunk spallation comes from the decohesion of the rust/substrate interface and usually occurs at the later stage of shot blast treatment.

(ii) Initially, the removed rust increases linearly with the number of impinged shots, before reaching a plateau value. The rate of derusting increases with the increase of

incident angle, impact velocity, and the shot diameter. The normal velocity has a larger influence on the derusting than the tangential velocity.

(iii) The ratio of the failed interface increases with the increase of the impact velocity and the shot diameter. On the contrary, a larger incident angle leads to a smaller ratio of failed interface.

(iv) The surface roughness is larger for a higher incident velocity, and/or a larger incident angle, and/or a larger shot diameter. The roughness is more sensitive to the normal velocity than to the tangential velocity. Both the maximum residual stress and the depth of compressive stress will become larger for a higher incident velocity, and/or a larger incident angle, and/or a larger shot diameter.

Acknowledgement: This work was supported by National Natural Science Foundation of China under Grant 11772231, Innovation Program of Shanghai Municipal Education Commission under Grant 15zz018, and the Fundamental Research Funds for the Central Universities under Grant 1500219095, and Shanghai Supercomputer Center.

References

Abaqus (2014): *Analysis User's Manual Version 6.14*. Dassault Systemes Simulia Corp.: Providence, RI, USA.

Banks-Sills, L. (2015): Interface fracture mechanics: theory and experiment. *International Journal of Fracture*, vol. 191, pp. 131-146.

Blackman, B. R. K.; Kinloch, A. J. (2001): Fracture tests for structural adhesive joints. In: Moore, D.; Pavan, A.; Williams, J. G. (Eds.), *Fracture Mechanics Testing Methods for Polymers, Adhesives and Composites*, pp. 225-267. Elsevier, Amsterdam.

Brannon, J. H.; Asmus, J. F. (1981): Citric acid augmented flashlamp cleaning of corroded steel surfaces. *Applications of Surface Science*, vol. 9, pp. 14-21.

Diehl, T. (2008a): On using a penalty-based cohesive zone finite element approach, Part I: Elastic solution benchmarks. *International Journal of Adhesion & Adhesives*, vol. 28, pp. 237-255.

Diehl, T. (2008b): On using a penalty-based cohesive zone finite element approach. Part II: Inelastic peeling of an epoxy-bonded aluminum strip. *International Journal of Adhesion & Adhesives*, vol. 28, pp. 256-265.

Gao, Y. K.; Wu, X. R. (2011): Experimental investigation and fatigue life prediction for 7475-T7351 aluminum alloy with and without shot peening-induced residual stresses. *Acta Materialia*, vol. 59, no. 9, pp. 3737-3747.

Griffin, D.; Daadbin, A.; Datta, S. (2004): The development of a three-dimensional finite element model for solid particle erosion on an alumina scale/MA956 substrate. *Wear*, vol. 256, pp. 900-906.

Guagliano, M. (2001): Relating Almen intensity to residual stresses induced by shot peening: a numerical approach. *Journal of Materials Processing Technology*, vol. 110, pp. 277-286.

Junkar, M.; Jurisevic, B.; Fajdiga, M.; Grah, M. (2006): Finite element analysis of single-particle impact in abrasive water jet machining. *International Journal of Impact Engineering*, vol. 32, no. 7, pp. 1095-1112.

Karac, A.; Blackman, B. R. K.; Cooper, V, Kinloch, A. J.; Sanchez, S. R. et al. (2011): Modeling the fracture behavior of adhesively-bonded joints as a function of test rate. *Engineering Fracture Mechanics*, vol. 78, pp. 973-989.

Kim, T.; Lee, H.; Hyun, H. C; Jung, S. (2013): Effects of Rayleigh damping, friction and rate-dependency on 3D residual stress simulation of angled shot peening. *Materials & Design*, vol. 46, pp. 26-37.

Kumar, N.; Shukla, M. (2012): Finite element analysis of multi-particle impact on erosion in abrasive water jet machining of titanium alloy. *Journal of Computational & Applied Mathematics*, vol. 236, no. 18, pp. 4600-4610.

Lebar, A.; Junkar, M. (2003): Simulation of abrasive waterjet machining based on unit event features. *Proceedings of the Institution of Mechanical Engineers Part B Journal of Engineering Manufacture*, vol. 217, no. 5, pp. 699-703.

Li, M. Z.; Liu, W. W.; Qing, X. C.; Yu, Y.; Liu, L. H. et al. (2016): Feasibility study of a new approach to removal of paint coatings in remanufacturing. *Journal of Materials Processing Technology*, vol. 234, pp. 102-112.

Lu, Y. L.; Brooks, C. R.; Chen, L. J.; Liaw, P. K.; Wang, G. Y. et al. (2005): A technique for the removal of oxides from the fracture surfaces of HAYNES 230 alloy. *Materials Characterization*, vol. 54, pp. 149-155.

Meguid, S. A.; Shagal, G.; Stranart, J. C. (2002): 3D FE analysis of peening of strain-rate sensitive materials using multiple impingement model. *International Journal of Impact Engineering*, vol. 27, pp. 119-134.

Mylonas, G. I.; Labeas, G. (2011): Numerical modelling of shot peening process and corresponding products: residual stress, surface roughness and cold work prediction. *Surface and Coatings Technology*, vol. 205, pp. 4480-4494.

Nguyen, T. T. H.; Bary, B.; De Larrard, T. (2015): Coupled carbonation-rust formation-damage modeling and simulation of steel corrosion in 3D mesoscale reinforced concrete. *Cement & Concrete Research*, vol. 74, pp. 95-107.

Oltra, R.; Yavas, O.; Cruz, F.; Boquillon, J. P.; Sartori, C. (1996): Modelling and Diagnostic of pulsed laser cleaning of oxidized metallic surfaces. *Applied Surface Science*, vol. 96-98, pp. 484-490.

Ouglova, A.; Berthaud, Y.; Francois, M.; Foct, F. (2006): Mechanical properties of an iron oxide formed by corrosion in reinforced concrete structures. *Corrosion Science*, vol. 48, no. 12, pp. 3988-4000.

Papini, M.; Spelt, J. K. (1997): Organic coating removal by particle impact. *Wear*, vol. 213, pp. 185-199.

Papini, M.; Spelt, J. K. (1998a): Indentation-induced buckling of organic coating. Part I: Theory and analysis. *International Journal of Mechanical Sciences,* vol. 40, pp. 1043-1059.

Papini, M.; Spelt, J. K. (1998b): Indentation-induced buckling of organic coating. Part II: Measurements with impacting particles. *International Journal of Mechanical Sciences*, vol. 40, pp. 1061-1068.

Papini, M.; Spelt, J. K. (1998c): The plowing erosion of organic coatings by spherical particles. *Wear*, vol. 222, pp. 38-48.

Park, K.; Paulino, G. H. (2011): Cohesive zone models: a critical review of Traction-Separation relationships across fracture surfaces. *Applied Mechanics Reviews*, vol. 64, pp. 1002.

Premack, T.; Douglas, A. (1995): Three-dimensional analysis of the impact fracture of 4340 steel. *International Journal of Solids and Structures*, vol. 32, no. 17, pp. 2793-2812.

Ramamurthi, M.; Lee, J. S.; Yang, S. H.; Kim, Y. S. (2013): Delamination characterization of bonded interface in polymer coated steel using surface based cohesive model. *International Journal of Precision Engineering & Manufacturing*, vol. 14, pp. 1755-1765.

Shipway, P. H.; Bromley, J. P. D.; Weston, D. P. (2007): Removal of coatings from polymer substrates by solid particle blasting to enhance reuse or recycling. *Wear*, vol. 263, pp. 309-317.

Society of Automotive Engineers (2001): *SAE Manual on Shot Peening, Fourth Edition*. SAE International, Warrendale, PA, USA.

Unal, O. (2016): Optimization of shot peening parameters by response surface methodology. *Surface and Coatings Technology*, vol. 305, pp. 99-109.

Wang, Y. F.; Yang, Z. G. (2008): Finite element model of erosive wear on ductile and brittle materials. *Wear*, vol. 265, pp. 871-878.

Wang, Z.; Zeng, X. Y.; Huang, W. L. (2003): Parameters and surface performance of laser removal of rust layer on A3 steel. *Surface and Coatings Technology*, vol. 166, pp. 10-16.

Yang, F.; Chen, Z.; Meguid, S. A. (2014): 3D FE modeling of oblique shot peening using a new periodic cell. *International Journal of Mechanics & Materials in Design*, vol. 10, pp. 133-144.

Yang, F.; Chen, Z.; Meguid, S. A. (2015): Effect of initial surface finish on effectiveness of shot peening treatment using enhanced periodic cell model. *International Journal of Mechanics & Materials in Design*, vol. 11, pp. 463-478.

Zhang, Q. C.; Ma, F.; Wu, J. S.; Zhazheng, W. L.; Chen, J. G. et al. (2002): Mechanical properties of native rust layer formed on a low alloy steel exposed in marine atmosphere. *Transactions of the Iron & Steel Institute of Japan*, vol. 42, no. 5, pp. 534-539.

Zouari, B.; Touratier, M. (2002): Simulation of organic coating removal by particle impact. *Wear*, vol. 253, pp. 488-497.